

Synthesis and application of Electrospun Nickel-Molybdenum/Graphene composite nanofibers and Nickel-Molybdenum nanofibers supported on Graphene nanosheets catalysts for hydrocracking of heavy hydrocarbons

Abstract

Electrospun NiMo/Graphene composite nanofibers (NMGF) and NiMo nanofibers supported on Graphene nanosheets (NMFG) were prepared via electrospinning technique and their performance for the hydrocracking of n-hexadecane (n-C₁₆) was compared with the NiMo/Graphene (NMG) synthesized by convectional impregnation method and commercial NiMo/ γ -Al₂O₃ (NMA) catalysts in a fixed-bed reactor. ICP, BET, TEM, FESEM, XRD, and NH₃-TPD tests were used to characterize the produced catalysts. The performance of the catalysts was evaluated based on total conversion and the distribution of liquid products over a continuous reaction period of 120 hours. The uniform dispersion of fibers, high surface area, large pore volume and more strong acidic sites of NMGF and NMFG catalysts resulted in the high percentage conversions of 99.5 and 99.2, respectively. The lighter hydrocarbons were achieved in hydrocracking using nanofibrous catalysts. Furthermore, nanofibrous catalysts produced a more stable catalyst than their counterparts, which suffered from coke production and deactivation of roughly 6% over 120 hours. The obtained results revealed the high potential of fibrous catalysts synthesized via electrospinning method compared with convectional metal oxide nanoparticles supported catalysts for hydrocracking of heavy oils.

Key words: Nano fibers, Nickel, Molybdenum, Graphene, Hydrocracking, Coke

1. Introduction

Conversion of heavy crude oil to valuable middle distillates has recently attracted by the industrial groups [1-12]. Among various methods including [gasification](#), [solvent extraction](#), [viscosity reduction](#), [coking and hydrocracking](#) (HC), the HC is the most suitable method for simultaneous conversion of heavy oils and vacuum residues into middle distillates and removal the impurities such as sulfur, nitrogen and metals [12-20]. The reactor system and catalyst properties play significant roles on the hydrocracking yield of heavy oils. Among various reactor systems including moving-bed, ebullated-bed and fixed-bed reactors (FBRs), the FBR system due to the simplicity of operation and easier scale-up is the most efficient reactor system for upgrading of heavy oils and residues [21-33]. [However, the main challenge of the fixed-bed hydrocracking reactor is the gradual decline in catalyst activity](#) [7]. Thus, the improvement in the catalyst lifetime and catalyst activity for increasing the middle distillates products from cracking of long chains paraffins is the main challenge [26, 27]. The metallic sites properties, the physico-chemical properties of the support such as pore diameter, and acidity, and their balance in the bifunctional catalyst should be considered for [decreasing the diffusion limitations and optimizing the catalyst activity toward hydrocracking of heavy oils](#) [11, 14, 30].

Various supports including zeolites [17, 20], metal organic frameworks [16], activated carbon[25], carbon nanotubes [5, 22, 28, 29,] and graphene [12, 31, 34, 35] have been used for the synthesis of supported metal catalysts. Among them, [the graphene nanosheets \(GNS\) have been utilized as a catalyst support in various catalytic applications due to their exceptional physicochemical stability and extensive surface area](#) [12, 35]. Furthermore, in recent studies, the activity of nanocatalysts was increased by converting of nanomaterials to the fibrous form via the electrospinning process [1]. [The electrospun nanofibrous catalysts shown significant activity for the hydrocracking of heavy oils because of their large surface area, low agglomeration, and ease](#)

of recovery [2]. The high surface area and low aggregation cause the high contents of active sites per mass of materials during hydrocracking of heavy oils [1, 36]. Recently, the zeolite nanofibers have been used as an efficient support for the cracking process. Anis et al synthesized the nickel oxide-tungsten oxide/zeolite nanofibers via electrospinning method for n-heptane hydrocracking [1]. The results indicated low coke formation with high conversion efficiency using nanofibers compared with performance of catalyst synthesized by the wet impregnation method. Anis et al was also investigate the potential of NiO-WO₃ over the Y-zeolite nanofibrous support for hydrocracking of n-heptane [2]. Kaminski et al. [8] investigated the hydrocracking of Athabasca vacuum residue using fibers composed of zeolite Y-NiO-WO₃ as the catalyst. Puron et al [21] compared the potential of NiMo catalyst over the alumina and carbon nanofibers supports for hydrocracking of a vacuum residue. Although, the relatively larger amounts of lighter products were obtained in the presence of Al₂O₃-supported catalyst, the coke formation was very low using carbon nanofiber-supported catalysts. To the best of our understanding, no research has been done on the synthesis of a NiMo/Graphene composite nanofibrous catalyst for hydrocracking of heavy oils.

In our previous works we studied hydro-cracking and hydro-treating of heavy hydrocarbons using Molybdenum based catalysts prepared by impregnation techniques and supported on conventional metal oxide and carbon materials [36,39-42]. In this work, NiMo/Graphene composite nanofibers and NiMo nanofibers supported on Graphene nanosheets were prepared via electrospinning process and their performances on the hydrocracking of n-hexadecane were compared with the Graphene supported NiMo catalyst and also with the industrial γ -Alumina supported NiMo catalysts synthesized by the wet impregnation method. The synthesized catalysts were analyzed

using ICP, BET, TEM, FESEM, NH_3 -TPD, and XRD techniques for characterization. The catalysts performance was studied in terms of their activity, liquid products selectivity and lifetime.

2. Experimental

2.1. Materials

Graphite fine powder for synthesis of graphene oxide was supplied from Sigma-Aldrich (Germany) Company. The commercial Ni-Mo/ $\gamma\text{-Al}_2\text{O}_3$ catalyst was sourced from the Bandar Abbas Oil Refinery (Iran). n-Hexadecane (used as the model feedstock component), nickel nitrate, and ammonium heptamolybdate were acquired from Merck. Polyvinylpyrrolidone (MWav: 130 kDa) for the synthesis of nanofibers was provided from Sigma-Aldrich (Germany) Company.

2.2. Synthesis of graphene oxide nanosheets

A modified Hummers process [6] was used to create graphene oxide (GO) from graphite fine powders. Briefly, 2 g graphite powders were dispersed into 50 mL $\text{HNO}_3\text{:H}_2\text{SO}_4$ mixture under sonication in an ultrasonic bath (Elma S40H, Germany) for 30 min to remove impurities. Then, 1 g NaNO_3 and 6 g KMnO_4 were added into the solution and sonication was continued for further 30 min. To terminate the reaction, the suspension was further treated with H_2O_2 to remove the residual KMnO_4 , followed by multiple washes with distilled water and subsequent drying in an oven at 80°C for 8 hours.

2.3. Synthesis of GO supported NiMo nanocatalysts

The NiMo/GO catalyst was synthesized via the impregnation method using $(\text{NH}_4)_2\text{MoS}_4$ and $\text{Ni}(\text{NO}_3)_2$ as the precursor salts. First, the predetermined amounts of Mo and Ni salts were dispersed in ethanol under sonication for 30 min. Then the support particles were dispersed into

the suspension under sonication for further 120 min. Then, the synthesized sample was centrifuged and dried in an oven at 80 °C for 12 h. After the impregnation process, the catalyst was calcined at 450 °C for 4 hours in an electrically heated quartz tube under a continuous N₂ flow of 50 mL min⁻¹. The composition of synthesized catalyst is presented on Table 1.

2.4. Synthesis of NiMo nanofibers over the GO support

The NiMo nanofibers were prepared via electrospinning method as described by Anis et al. [2]. Briefly, 10 wt.% PVP solution was prepared by dissolving 1 g PVP in ethanol for 2 h. Then, the prepared NiMo salts suspension (PVP/salts v:v 1:1) was added into the PVP solution under stirring for further 12 h to obtain a homogeneous solution of PVP/salts. The applied voltage, tip-collector distance, flow rate and collector speed were 22 kV, 12 cm, 0.5 mL/h and 1000 rpm, respectively for fabrication of PVP/salts nanofibers. The electrospun fibers were calcined at 550 °C at a rate of 2 °C/min and kept there for two hours in order to remove the polymeric phase and break down the metal precursors at the same time. The synthesized fibers were dispersed into the GO suspension under stirring for 4 h. Then, the synthesized sample was centrifuged and dried in an oven at 80 °C for 12 h. The synthesized catalyst's composition is shown in Table 1.

2.5. Synthesis of NiMo/GO composite nanofibrous catalyst

The NiMo/GO nanofibrous catalyst was prepared via electrospinning process in the presence of PVP. To prevent the agglomeration of nanosheets, the prepared GO/salts suspension were dropwisely added into the PVP solution and sonication was continued for further 3 h. Then, the PVP/GO/salts solution was transferred into the syringe with needle gauge of 19 for electrospinning process. The applied voltage, tip-collector distance, flow rate and collector speed were constant at

22 kV, 12 cm, 0.5 mL/h and 1000 rpm, respectively. The composition of synthesized catalyst is presented on Table 1.

2.6. Catalysts characterization

The Varian VISTA-MPX inductively coupled plasma-optical emission spectrometry (ICP-OES) equipment was used to assess the concentration of Ni and Mo metals on the catalysts. BET surface area pore volume, and pore diameter of synthesized catalysts were measured using N₂ physisorption at 77 K in ASAP-2010 Micromeritics system. The X-ray diffraction (XRD) analysis was performed utilizing a Philips PW1840 diffractometer equipped with monochromatized Cu/K α radiation. The measurements were carried out over an angular range of 10–80° under scanning speed of 0.03° (2 θ) s⁻¹. The half-width of a selected peak was entered into the Debye-Scherrer equation to get the crystallite diameter. The morphological characteristics of synthesized catalysts were conducted using field emission electron microscope (FESEM, Hitachi S-4160) and transmission electron microscope (TEM) (Philips). Image-Proplus software from Media Cybernetics was used to measure the particle size distribution. The particle size distribution was created by measuring the particle sizes of at least 20 randomly chosen segments. The acidity of the synthesized catalysts were evaluated using temperature-programmed desorption of ammonia (NH₃-TPD) on a chemisorption physisorption analyzer (ChemBET Pulsar TPR/TPD, Quantachrome). 200 mg of catalyst sample was pretreated at 500 °C for 3 hours. After the temperature was reduced to 50 °C, ammonia adsorption was conducted for 40 minutes. Any excess ammonia was then purged using helium at 50 °C for 2 hours. Finally, NH₃-TPD analysis was performed by heating the samples from 50 to 550 °C at a rate of 10 °C.min⁻¹, with a helium flow rate of 15 mL.min⁻¹.

The coke/carbon deposits on the spent catalysts were measured by a common combustion method in a carbon analyzer multi EA 2000 using a high-grade NDIR detector (Analytik Jena AG).

2.7. Reaction testing and analysis

The hydrocracking of n-hexadecane was carried out in a stainless steel fixed-bed tubular reactor, as illustrated in Figure 1. Each experiment involved loading 2 grams of catalyst into the reactor, followed by reduction using hydrogen gas at a pressure of 30 bar and a space velocity of 600 h^{-1} . The temperature was gradually increased from ambient to 453 K at a heating rate of $0.5 \text{ K}\cdot\text{min}^{-1}$ and then maintained at this level for 1 hour. The catalysts were then subjected to a sulfidation process using a stream of 1 wt.% dimethyl disulfide in hexane, operating at a liquid hourly space velocity (LHSV) of 2 h^{-1} , a hydrogen pressure of 30 bar, and a hydrogen-to-oil volumetric ratio (H_2/Oil) of 80 nl/L to facilitate the formation of Ni-Mo-S active phases. The catalyst samples were subsequently heated from 453 K to 533 K at a rate of 0.5 K/min, followed by further heating from 533 K to 583 K at a rate of 2 K/min. The hydrocracking of n-hexadecane was then carried out at this temperature for 120 hours, during which the catalytic performance was evaluated. The reaction conditions included a temperature of 583 K, an $\text{H}_2/\text{n-hexadecane}$ ratio of 175 nl/L, a pressure of 45 bar, and an LHSV of 1.4 h^{-1} .

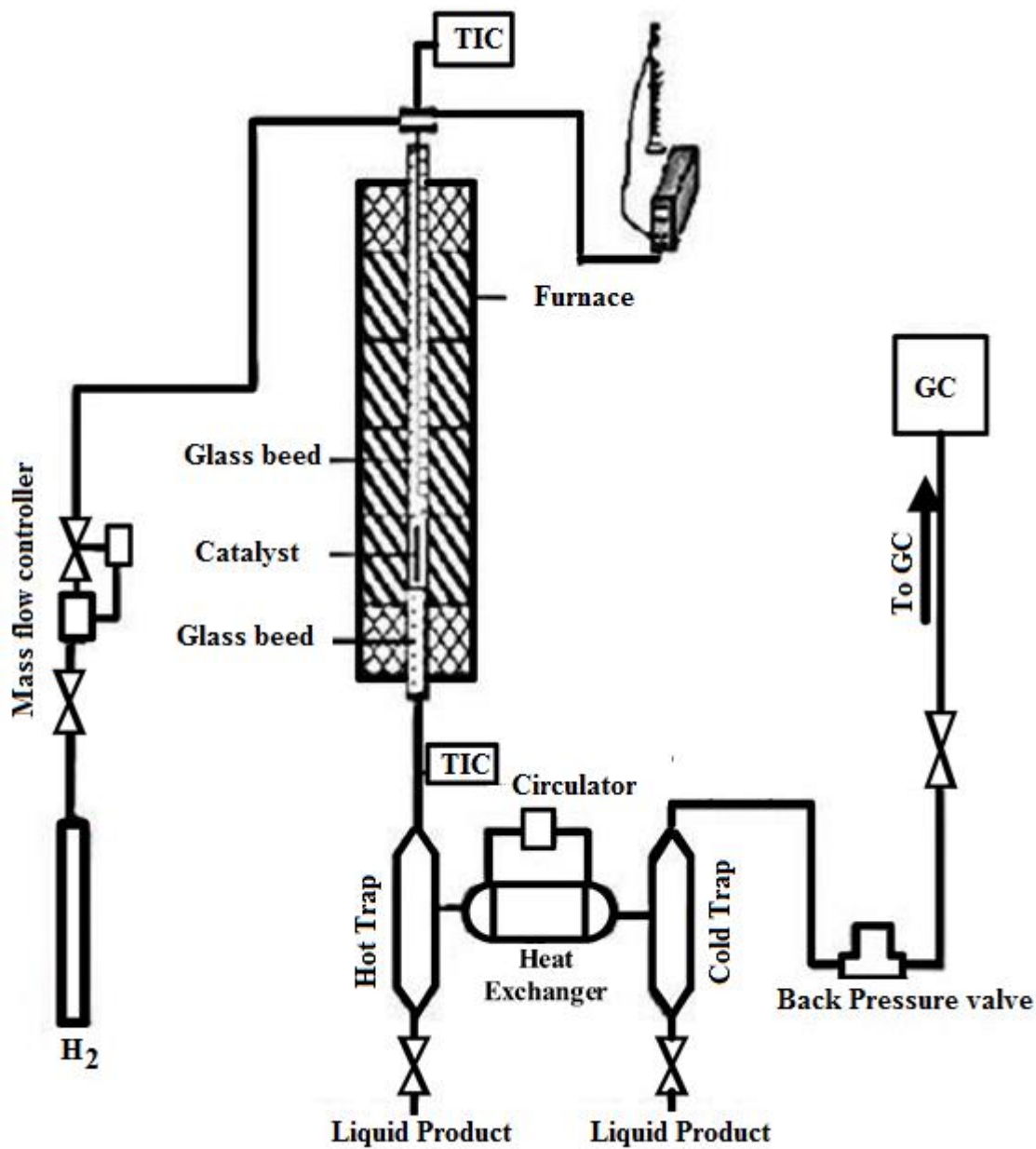


Figure 1: The schematic of the experimental setup

The liquid products were collected every 12 h and analyzed using gas chromatography (Agilent 7890A), mass spectrometer (5975C VL MSD with triple-axis detector) equipped with a capillary column (Rtx 5 MS, HT-30 m long, 25 μ m film thickness). The percentage conversion of n-hexadecane and hydrocracking products yield were calculated as follows:

$$\text{Conversion}_{n-C16}(\%) = \left(1 - \frac{(n - C16 \text{ content})_{out}}{(n - C16 \text{ content})_{in}}\right) \times 100 \quad (1)$$

$$\text{Yield}(\%) = \frac{(\text{Content of hydrocracking product formed})}{(n - C16 \text{ content})_{in}} \times 100 \quad (2)$$

3. Results and discussion

3.1. Characterization of synthesized catalysts

The physico-chemical properties of synthesized catalysts and industrial catalyst are presented in Table 1. As shown, the Ni/(Ni+Mo) ratios are about ~0.3 for all the catalysts (ICP results). Table 1 shows that, the BET surface area and pore volume of nanofibrous catalysts were higher than that of NiMo nanoparticles coated graphene nanosheets. The low surface area and pore volume in the case of NiMo/GNS catalyst may be attributed to the more agglomeration of NiMo particles and pores blockage compared with nanofibrous catalysts. The fibrous structure of NiMo fibers/GNS and NiMo/GNS fibers catalyst can improve the mass transfer properties between the acidic and the metal sites which facilitate the diffusion of reactants and promise the high activity of nanofibrous catalysts for hydrocracking process. Both the surface area and pore volume are noticeably lower in the case of industrial alumina supported catalyst.

Table 1: Textural properties and chemical composition of synthesized catalysts

Catalyst/ support	Abbreviation	Ni (wt.%)	Mo (wt.%)	S _{BET} (m ² /g)	V _{total} (Cm ³ /g)	d _{avr} (nm)
NiMo/ Al ₂ O ₃	NMA	3.7	9.2	215	0.356	9.8
NiMo/GNS	NMG	3.5	8.8	542	0.565	2.15
NiMo fibers/GNS	NMFG	3.6	8.9	652	0.765	1.15

NiMo/GNS fibers	NMGF	3.7	9.1	824	0.925	0.89
-----------------	------	-----	-----	-----	-------	------

The XRD patterns of Graphene, NMG, NMFG and NMGF catalysts are illustrated in Figure 2. The main diffraction peak observed at $2\theta = 23.3$ and 27.1° could be attributed to the (1 1 0) and (0 2 1) planes of MoO_3 orthorhombic phase in the NMFG and NMGF catalysts. The observed weak peak at $2\theta = 37.3^\circ$ was due to the (4 0 0) plane of NiMoO_4 monoclinic phase. The XRD analysis indicated the presence of MoO_3 as major phase compared with NiO as a minor phase in the NMFG catalyst. The weak diffraction peak for NiO was detected at $2\theta = 43.4^\circ$. A prominent reflection peak at $2\theta = 26^\circ$ was assigned to graphitic carbon. Furthermore, the XRD diffraction patterns of the catalysts showed the more crystallite reflections of Mo or Ni metal oxides for nanofibrous catalysts compared with the NMG which may be attributed to the uniform dispersion of fibers on the Graphene matrix compared with NiMo particles.

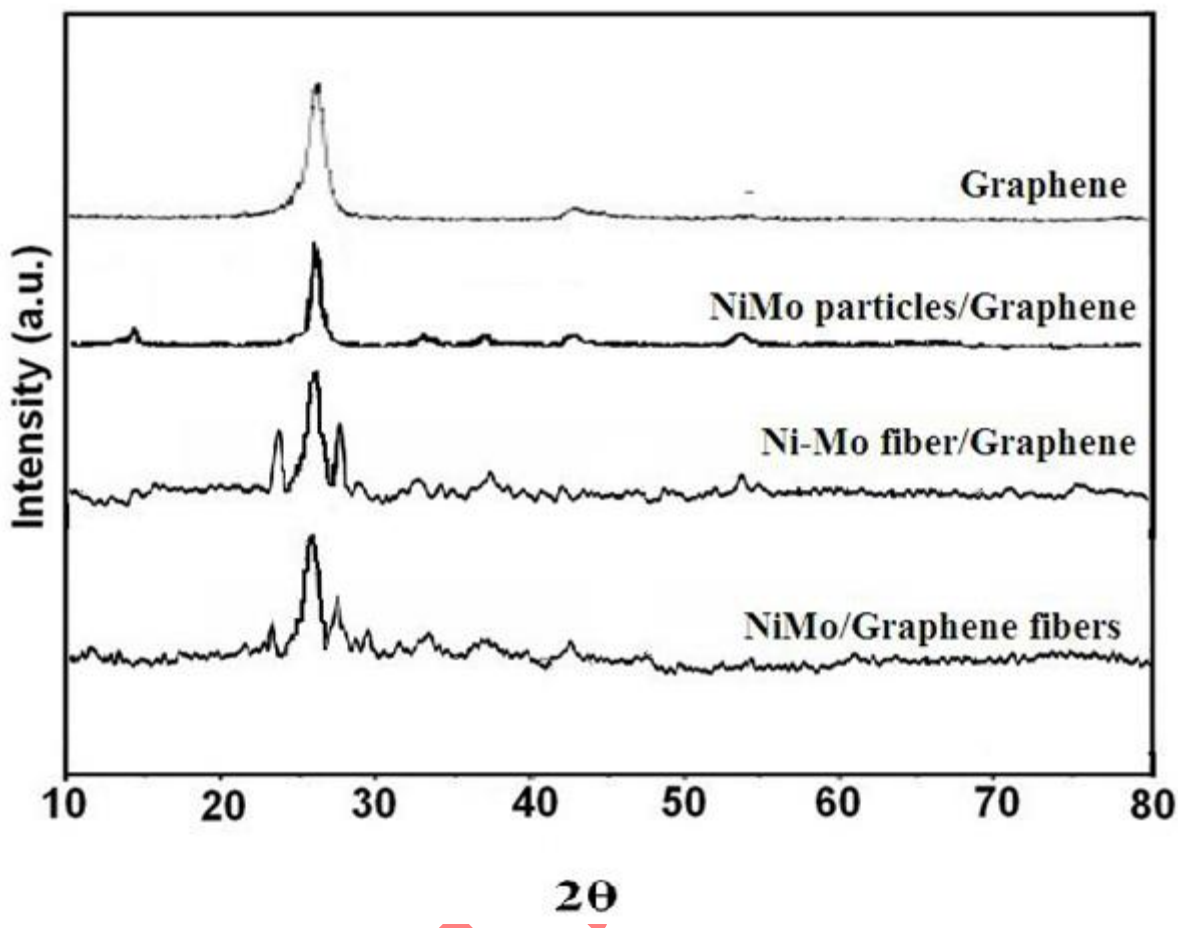


Figure 2. XRD patterns of Graphene, NMG, NMFG and NMGF catalysts

The surface morphologies of the NMG, NMFG and NMGF and particle/fiber size distribution are illustrated in Figures 3. The TEM image of NMG revealed a high dispersion of NiMo particles across the surface of the NMG catalyst, as shown in Figure 3a. The dark spots could be attributed to the attaching of the NiMo particles to the Graphene surface support. As shown, Graphene channels have restricted the growth of the particles. Also, Figure 3a illustrates the size distribution of the metal particles, which is calculated using data from four TEM images (one of which is presented in this manuscript) and the population of about 100 metal particles of catalysts. A narrow nanoparticle size distribution on graphene is depicted in this figure and the TEM images. The size distribution of the particles was ranging from 2-7 nm.

As shown in Figure 3b, the smooth NiMo fibers without any beads ranging from 20 to 100 nm with average diameter of 67 nm were produced on the graphene nanosheets surface. The uniform fibers with higher fiber diameter were obtained for NiMo/GNS fibers (Figure 3c). The fiber diameter distribution was in the range 50-250 nm with an average diameter of 160 nm.

Accepted Manuscript

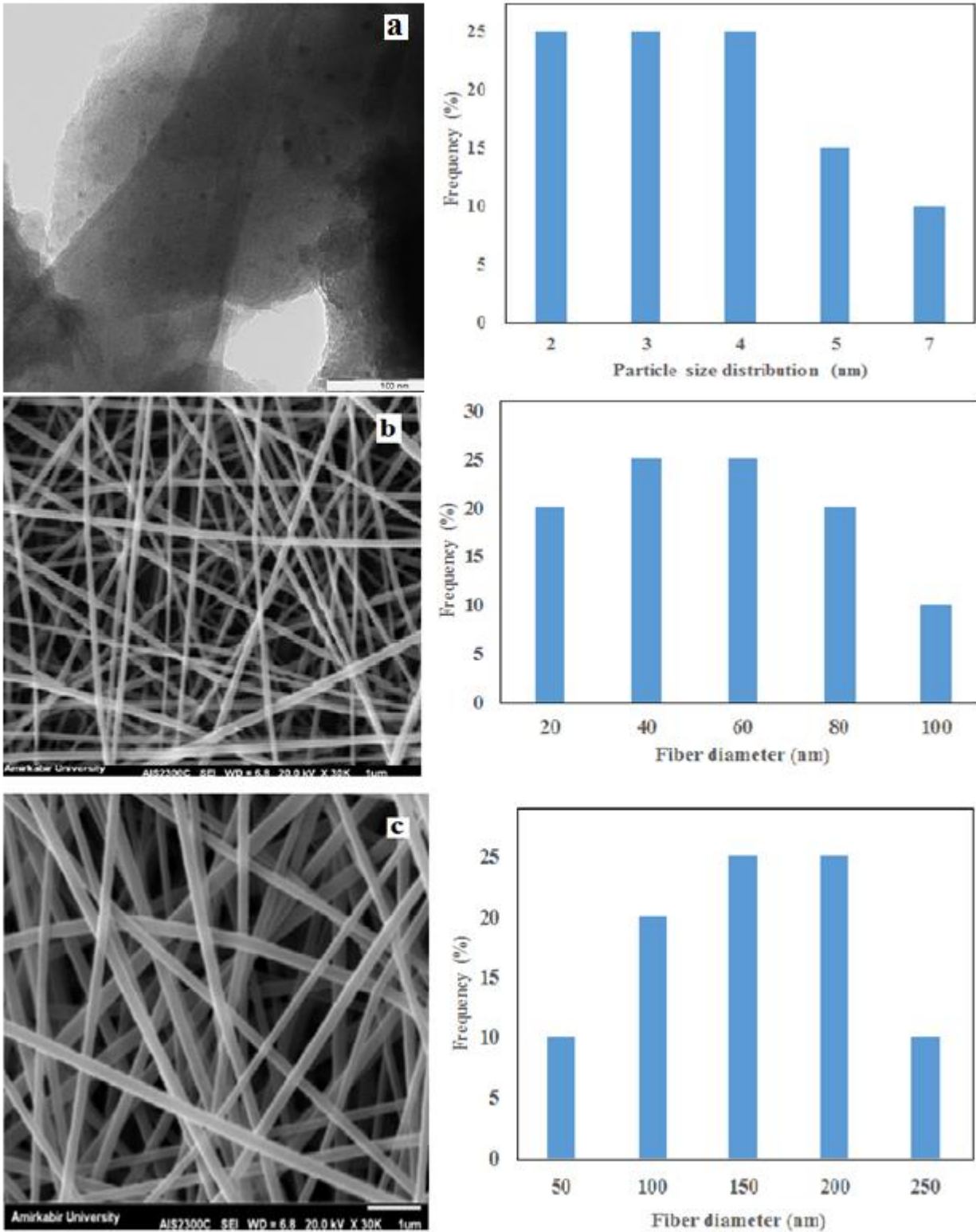


Figure 3. (a) TEM image and particle size distribution of NMG, (b), (c) FESSEM images and particle size distributions of NMFG and NMGF catalysts.

The NH₃-TPD profiles of synthesized catalysts are depicted in Figure 4. The acid sites distributions of the catalysts are also displayed in Table 2. The synthesized catalysts showed different distributions of acidic sites (weak, medium and strong acidic sites were considered for temperatures lower than 200 °C, between 200 and 400 °C and higher than 400 °C). The NMFG and NMGF nanofibrous catalysts with total acidity of 521.4 and 563.8 μmolg⁻¹ had enough acidic sites for n-hexadecane cracking which could be attributed to the high surface area and large pore volume of fibrous catalysts compared with NMG catalyst with total acidity of 186.6 μmolg⁻¹. The reduced diffusion and adsorption of NH₃ molecules from the NMG catalyst's pores may be the cause of the catalyst's decreased acidity. The order of the number of strong acidic sites is NMGF>NMFG>NMG.

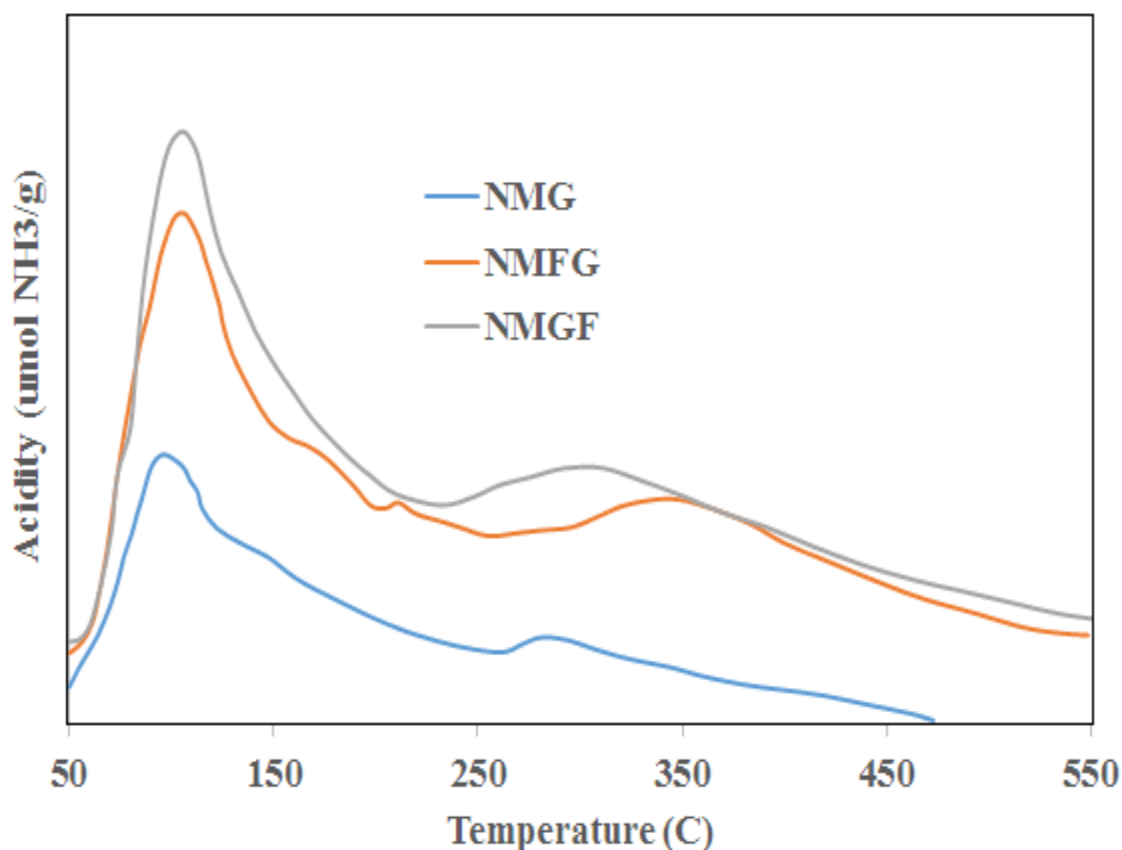


Figure 4. NH₃-TPD profiles of synthesized NMG, NMFG and NMGF

Table 2. Acid sites distribution in the synthesized catalysts

Catalyst	NH ₃ content (μmol/g catalyst)			Total acid site
	Weak acid site	Medium acid site	Strong acid site	
NMG	76.9	76.4	33.3	186.6
NMFG	216.1	189.9	115.4	521.4
NMGF	240.1	200.4	123.3	563.8

3.2. Performance of synthesized catalysts on C₁₆ hydrocracking

The total conversion and products selectivity for commercial NiMo/γ-Al₂O₃ catalyst and synthesized NMG, NMFG and NMGF catalysts have been investigated for 120 h. The results for the first 12 h synthesis are illustrated in Table 3. As shown, only 63% conversion was observed for commercial NiMo/γ-Al₂O₃ catalyst. Whereas, 85.1, 99.2 and 99.5% total conversion of n-C₁₆ were achieved using NMG, NMFG and NMGF catalysts, respectively. The synthesized nanofibrous catalysts showed the higher conversion of n-C₁₆ compared with NMG catalyst. This behavior may be attributed to the uniform dispersion of fibers compared with dispersion of nanoparticles on the Graphene nanosheets with some agglomeration of NiMo particles as described by TEM and FESEM images. The hydrocracking of n-C₁₆ consisting the hydrogenation at metal sites followed by cracking at acidic sites of support were occurred. The better balance between metal sites of NiMo and acid sites of graphene supports led to high cracking and hydrogenation activity of synthesized catalysts. The strong acid sites of supports of NMG, NMFG, and NMGF catalysts resulted in the high conversion of synthesized catalysts for n-C₁₆ hydrocracking. Furthermore, increasing the surface area enhanced the accessibility of feed molecules to the catalyst's active sites.

Table 3. Percentage conversion and products yield in the presence of different catalysts

Catalyst	Conversion (%)	Gaseous Products (%)	Liquid Products (%)
NMA	63	4.3	95.7
NMG	85.1	5.4	94.6
NMFG	99.2	7.9	92.1
NMGF	99.5	8.4	91.6

The products yield during the first 12 h n-C₁₆ hydrocracking is also presented on Table 3. Comparing the results of the synthesized NMG, NMFG, and NMGF catalysts with the results obtained from industrial catalyst demonstrates that the quantity of gaseous products rises while the quantity of liquid products reduces. The support porosity, the number and strength of acid sites, and the distance between the two catalytic functions are some of the variables that can affect the catalyst's selectivity in the hydrocracking process. The cracking significantly influences by the strength of the individual type of sites rather than total concentration. The cracking mainly takes place on Brønsted acid sites. The cracking ability of catalysts follows the same trend as the Brønsted acidity. However, in a bifunctional catalyst, the balance between its two catalytic functions plays a crucial role in determining its overall performance. Enhancing the hydrogenation capability (which takes place on the metal sites of NiMo) can lead to a notable improvement in selectivity toward light products. This occurs by accelerating the desorption rate of carbocations, thereby minimizing the extent of secondary cracking on NMG, NMFG, and NMGF catalysts. The distributions of liquid hydrocarbon products from hydrocracking of n-hexadecane using synthesized NMG, NMFG, NMGF and NMA catalysts are presented in Figure 5. Also, the distribution of the C₆ isomers (n-hexane (nC₆), 2-methylpentane (2MP), 3-methylpentane (3MP), 2,3-dimethylbutane (23DMB), and 2,2-dimethylbutane (22DMB)) for the reaction with NMGF

catalyst is shown on the left corner of this figure. Due to the high partial pressure of hydrogen in the reactor, most of the C_6 isomers are saturated hydrocarbons. As indicated, the main liquid hydrocarbon component produced during the hydrocracking of n- C_{16} using NMGF, NMFG and NMGF catalysts were C_5 - C_{12} alkanes. The appropriate balance between the textural and acidic properties of nanofibrous catalysts resulted in the selective hydrocracking of n- C_{16} .

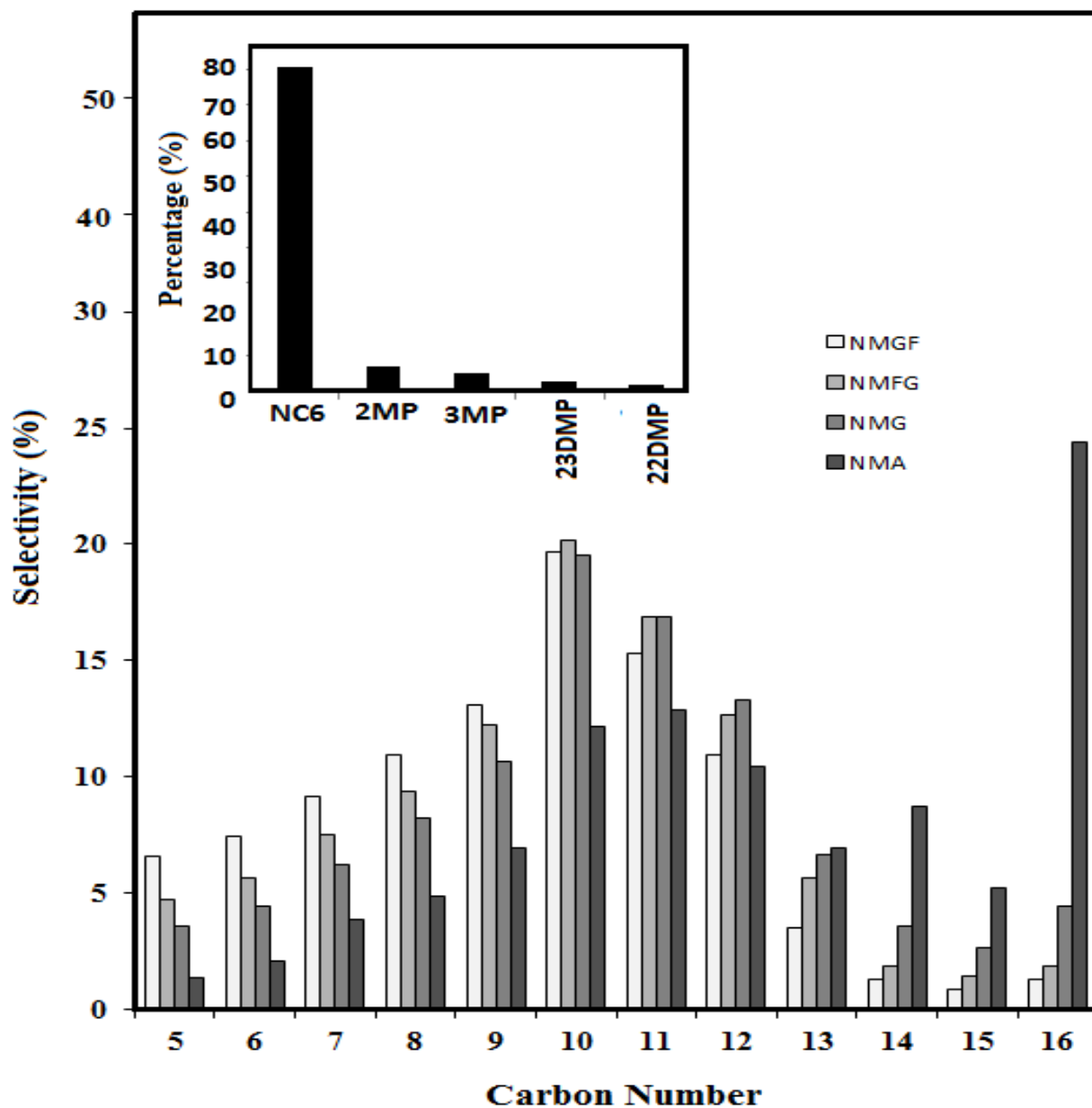


Figure 5. Liquid hydrocarbon products distribution from hydrocracking of n-hexadecane

Figure 6 shows the percentage conversion variations with the duration of reaction for different catalysts. This figure shows that the catalysts displayed different stability pattern within a time period of 120 h continues n-C₁₆ hydrocracking. In the case of commercial NMA catalyst, 120 h continues reaction decreased the percentage conversion from to 63 to 56.6 (6.4% decrease). The %conversion severely decreased in the first day and then leveled off. The decrease for NMG, NMFG and NMGF catalysts were 5.5, 2.3 and 1.9% respectively. The commercial and NMG catalysts were deactivated by time significantly but, complete almost conversion of n-C₁₆ took place by the nanofibrous catalysts.

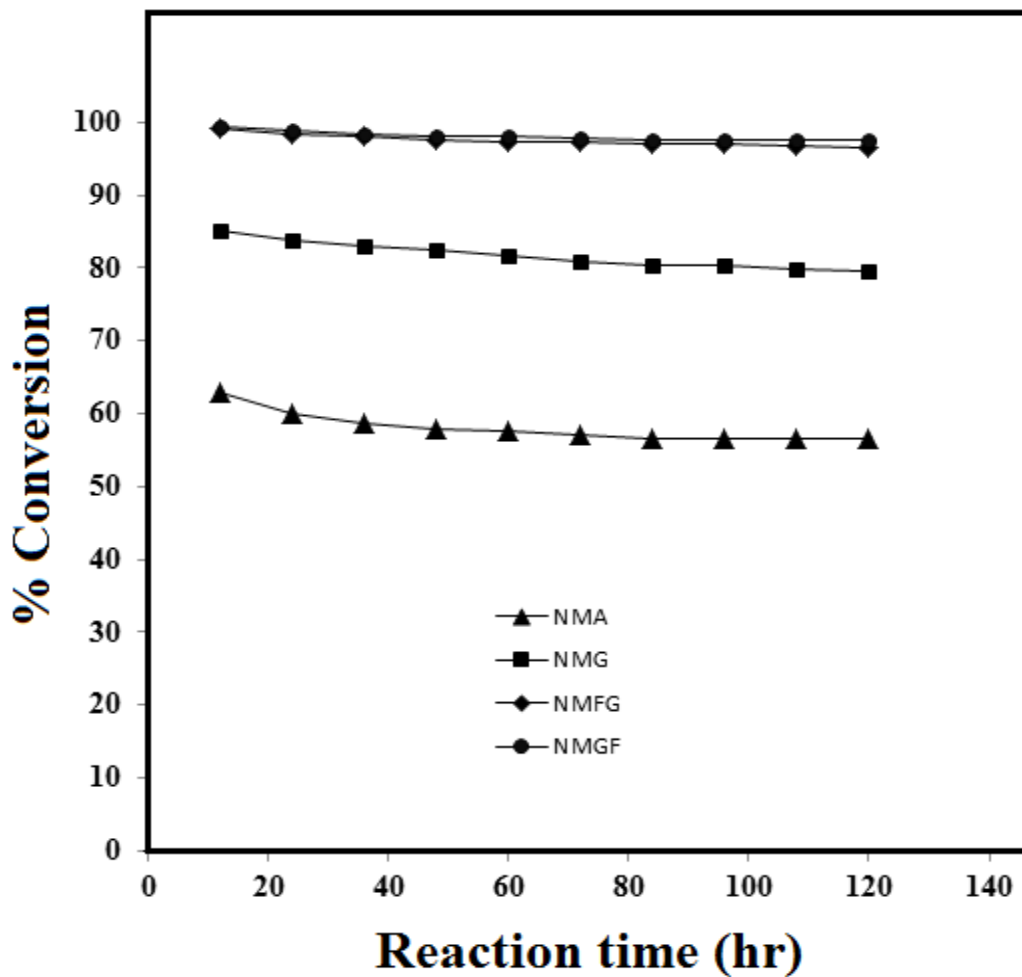


Figure 6. Variations of %Conversion with time for different catalysts

The more coke formation during hydrocracking of n-C₁₆ could be responsible for deactivation of commercial NMA and NMG catalysts. Table 4 shows the percentage of coke deposits during n-C₁₆ hydrocracking. The coke formation on the catalyst can be resulted in the catalyst deactivation via the coke deposits in the catalyst pores and catalyst surface and following the blocking of pores and surface area loss. On the other hand, the reduction in the activity of catalyst take place through the non-volatile carbonaceous deposits that incorporate into the pores of catalyst or adsorb on the catalyst surface. The catalyst properties such as acidity, surface area and pore size distribution can affect on the coke deposition. As shown, the minimum coke deposition was obtained for NMGF nanofibrous catalyst. The faster kinetic of hydrocracking process using nanofibrous catalysts may lead to fewer coke deposits. Furthermore, the higher surface area of catalyst and the larger intra-fiber distance (large pore volume) could be responsible for the lower coke formation on the catalyst. The low coke formation can reduce the loss of liquid products and increase the production of variable products via hydrocracking of heavy oils.

Table 4: Percentage of coke deposition during n-C₁₆ hydrocracking using different catalysts

Catalyst/ support	Coke (%)
NiMo/ Al ₂ O ₃	1.85
NiMo/GNS	0.45
NiMo fibers/GNS	0.25
NiMo/GNS fibers	0.22

Using the catalyst prepared in this research in the existing industrial reactors, due to its higher activity and productivity, will increase the production of lighter products, especially middle

distillation products. Also, the use of this catalyst in the design of new hydrocracking plants will reduce the size of the reactor. Both of the above cases will improve the economic aspects of the hydrocracking plants. In addition, increasing the lifetime of the catalyst and reducing the production of coke on the catalyst will increase the exploitation period and continuous operation time on stream of the reactor, and this issue will also have positive effects on the economic factors of the process.

4. Conclusion

Nanofibrous catalysts were successfully developed for hydrocracking of heavy oils in a fixed bed reactor. The characteristic of synthesized nanofibrous catalysts indicated the high surface area, large pore volume and more strong acidic sites. The synthesized fibrous catalysts exhibited more catalyst activity for hydrocracking compared with NiMo nanoparticles coated graphene and commercial NiMo/Al₂O₃ catalyst. The lighter hydrocarbons were achieved in hydrocracking using nanofibrous catalysts. Nanofibrous catalysts resulted in a more stable catalyst, compared with their counterparts.

Abbreviation

NMGF: Nickel Molybdenum/Graphene composite nanofibers

NMFG: Nickel Molybdenum nanofibers supported on Graphene nanosheets

NMA: Nickel Molybdenum /Al₂O₃

NMG: Nickel Molybdenum/Graphene

ICP: Inductively Coupled Plasma

FESEM: Field Emission Scanning Electron Microscope

TEM: Transmission Electron Microscopy

XRD: X-ray Diffraction

FBR: Fixed-Bed Reactors

GNS: graphene nanosheets

NH₃-TPD: Temperature-Programmed Desorption of Ammonia

References

- [1] Anis S F, Singaravel G and Hashaikh R (2017) Electropun Ni-W/zeolite composite fibers for n-heptane hydrocracking and hydroisomerization. *Materials Chemistry and Physics*, 200146-154. <https://doi.org/https://doi.org/10.1016/j.matchemphys.2017.07.081>
- [2] Anis S F, Singaravel G and Hashaikh R (2018) Hierarchical nano zeolite-Y hydrocracking composite fibers with highly efficient hydrocracking capability. *RSC advances*, 830: 16703-16715. <https://doi.org/DOI: 10.1039/C8RA02662A>
- [3] Bouchy C, Hastoy G, Guillon E and Martens J (2009) Fischer-Tropsch waxes upgrading via hydrocracking and selective hydroisomerization. *Oil & Gas Science and Technology-Revue de l'IFP*, 641: 91-112. <https://doi.org/DOI: 10.2516/ogst/2008047>
- [4] Chang J, Tsubaki N and Fujimoto K (2001) Elemental sulfur as an effective promoter for the catalytic hydrocracking of Arabian vacuum residue. *Fuel*, 8011: 1639-1643. [https://doi.org/https://doi.org/10.1016/S0016-2361\(01\)00035-7](https://doi.org/https://doi.org/10.1016/S0016-2361(01)00035-7)
- [5] Kayukova G, Mikhailova A, Kosachev I, Feoktistov D A and Vakhin A (2018) Conversion of heavy oil with different chemical compositions under catalytic aquathermolysis with an amphiphilic Fe-Co-Cu catalyst and kaolin. *Energy & fuels*, 326: 6488-6497. <https://doi.org/https://doi.org/10.1021/acs.energyfuels.8b00347>
- [6] Chuan L, Bin S, Min C, SHANG H-y and QUE G-h (2007) Application of Co-Mo/CNT catalyst in hydro-cracking of Gudao vacuum residue. *Journal of Fuel Chemistry and Technology*, 354: 407-411. [https://doi.org/https://doi.org/10.1016/S1872-5813\(07\)60026-7](https://doi.org/https://doi.org/10.1016/S1872-5813(07)60026-7)
- [7] Hummers Jr W S and Offeman R E (1958) Preparation of graphitic oxide. *Journal of the american chemical society*, 806: 1339-1339. <https://doi.org/https://doi.org/10.1021/ja01539a017>

- [8] Kalbasi R J, Massah A R and Barkhordari Z (2010) An efficient and green approach for the esterification of aromatic acids with various alcohols over H₃PO₄/TiO₂-ZrO₂. *Bulletin of the Korean Chemical Society*, 318: 2361-2367. <https://doi.org/https://doi.org/10.5012/bkcs.2010.31.8.2361>
- [9] Kaminski T, Anis S F, Husein M M and Hashaikheh R (2018) Hydrocracking of athabasca VR using NiO-WO₃ zeolite-Based catalysts. *Energy & Fuels*, 322: 2224-2233. <https://doi.org/https://doi.org/10.1021/acs.energyfuels.7b03754>
- [10] Kham-or P, Suwannasom P and Ruangviriyachai C (2016) Effect of agglomerated NiMo HZSM-5 catalyst for the hydrocracking reaction of *Jatropha curcas* oil. *Energy Sources, Part A: Recovery, Utilization, and Environmental Effects*, 3824: 3694-3701. <https://doi.org/https://doi.org/10.1080/15567036.2016.1166165>
- [11] Kim H, Nguyen-Huy C and Shin E W (2014) Macroporous NiMo/alumina catalyst for the hydrocracking of vacuum residue. *Reaction Kinetics, Mechanisms and Catalysis*, 1132: 431-443. <https://doi.org/https://doi.org/10.1007/s11144-014-0764-5>
- [12] Kim S K, Yoon D, Lee S-C and Kim J (2015) Mo₂C/graphene nanocomposite as a hydrodeoxygenation catalyst for the production of diesel range hydrocarbons. *ACS Catalysis*, 56: 3292-3303. <https://doi.org/https://doi.org/10.1021/acscatal.5b00335>
- [13] Kim Y-S, Yun G-N and Lee Y-K (2014) Novel Ni₂P/zeolite catalysts for naphthalene hydrocracking to BTX. *Catalysis Communications*, 45: 133-138. <https://doi.org/https://doi.org/10.1016/j.catcom.2013.11.010>
- [14] Lee J, Choi Y, Shin J and Lee J K (2016) Selective hydrocracking of tetralin for light aromatic hydrocarbons. *Catalysis Today*, 265: 144-153. <https://doi.org/https://doi.org/10.1016/j.cattod.2015.09.046>
- [15] Liang J, Liang Z, Zou R and Zhao Y (2017) Heterogeneous catalysis in zeolites, mesoporous silica, and metal-organic frameworks. *Advanced Materials*, 2930: 1701139. <https://doi.org/https://doi.org/10.1002/adma.201701139>
- [16] Liu J, He J, Wang L, Li R, Chen P, Rao X, Deng L, Rong L and Lei J (2016) NiO-PTA supported on ZIF-8 as a highly effective catalyst for hydrocracking of *Jatropha* oil. *Scientific reports*, 61: 1-11. <https://doi.org/https://doi.org/10.1038/srep23667>
- [17] Manrique C, Guzmán A, Pérez-Pariente J, Márquez-Álvarez C and Echavarría A (2016) Vacuum gas-oil hydrocracking performance of Beta zeolite obtained by hydrothermal synthesis using carbon nanotubes as mesoporous template. *Fuel*, 182: 236-247. <https://doi.org/https://doi.org/10.1016/j.fuel.2016.05.097>
- [18] Morel F, Kressmann S, Harlé V and Kasztelan S (1997) Processes and catalysts for hydrocracking of heavy oil and residues. In *Studies in surface science and catalysis Vol. 106*, pp. 1-16. Elsevier. [https://doi.org/https://doi.org/10.1016/S0167-2991\(97\)80003-1](https://doi.org/https://doi.org/10.1016/S0167-2991(97)80003-1)

- [19] Okunev A, Parkhomchuk E V e, Lysikov A I, Parunin P D, Semeykina V and Parmon V N (2015) Catalytic hydroprocessing of heavy oil feedstocks. *Russian chemical reviews*, 849: 981. <https://doi.org/DOI.10.1070/RCR4486>
- [20] Park K-C and Ihm S-K (2000) Comparison of Pt/zeolite catalysts for n-hexadecane hydroisomerization. *Applied Catalysis A: General*, 2032: 201-209. [https://doi.org/https://doi.org/10.1016/S0926-860X\(00\)00490-7](https://doi.org/https://doi.org/10.1016/S0926-860X(00)00490-7)
- [21] Purón H, Pinilla J, Suelves I and Millan M (2015) Acid treated carbon nanofibers as catalytic support for heavy oil hydroprocessing. *Catalysis Today*, 24979-85. <https://doi.org/https://doi.org/10.1016/j.cattod.2014.09.021>
- [22] Rad M R, Rashidi A, Vafajoo L and Rashtchi M (2014) Preparation of Co–Mo supported multi-wall carbon nanotube for hydrocracking of extra heavy oil. *Journal of Industrial and Engineering Chemistry*, 206: 4298-4303. <https://doi.org/https://doi.org/10.1016/j.jiec.2014.01.036>
- [23] Rana M S, Sámano V, Ancheyta J and Diaz J (2007) A review of recent advances on process technologies for upgrading of heavy oils and residua. *Fuel*, 869: 1216-1231. <https://doi.org/https://doi.org/10.1016/j.fuel.2006.08.004>
- [24] Sahu R, Song B J, Im J S, Jeon Y-P and Lee C W (2015) A review of recent advances in catalytic hydrocracking of heavy residues. *Journal of Industrial and Engineering Chemistry*, 2712-24. <https://doi.org/https://doi.org/10.1016/j.jiec.2015.01.011>
- [25] Subsadsana M, Sansuk S and Ruangviriyachai C (2018) Enhanced liquid biofuel production from crude palm oil over synthesized NiMoW-ZSM-5/MCM-41 catalyst. *Energy Sources, Part A: Recovery, Utilization, and Environmental Effects*, 402: 237-243. <https://doi.org/https://doi.org/10.1080/15567036.2017.1411992>
- [26] Sun C, Zhan T, Pfeifer P and Dittmeyer R (2017) Influence of Fischer-Tropsch synthesis (FTS) and hydrocracking (HC) conditions on the product distribution of an integrated FTS-HC process. *Chemical Engineering Journal*, 310272-281. <https://doi.org/https://doi.org/10.1016/j.cej.2016.10.118>
- [27] Taylor R J and Petty R H (1994) Selective hydroisomerization of long chain normal paraffins. *Applied Catalysis A: General*, 1191: 121-138. [https://doi.org/https://doi.org/10.1016/0926-860X\(94\)85029-1](https://doi.org/https://doi.org/10.1016/0926-860X(94)85029-1)
- [28] Trépanier M, Tavasoli A, Dalai A K and Abatzoglou N (2009) Co, Ru and K loadings effects on the activity and selectivity of carbon nanotubes supported cobalt catalyst in Fischer–Tropsch synthesis. *Applied Catalysis A: General*, 3532: 193-202. <https://doi.org/https://doi.org/10.1016/j.apcata.2008.10.061>
- [29] Trépanier M, Tavasoli A, Dalai A K and Abatzoglou N (2009) Fischer–Tropsch synthesis over carbon nanotubes supported cobalt catalysts in a fixed bed reactor: Influence of acid treatment. *Fuel Processing Technology*, 903: 367-374. <https://doi.org/https://doi.org/10.1016/j.fuproc.2008.10.012>

- [30] Upare D P, Park S, Kim M, Jeon Y-P, Kim J, Lee D, Lee J, Chang H, Choi S and Choi W (2017) Selective hydrocracking of pyrolysis fuel oil into benzene, toluene and xylene over CoMo/beta zeolite catalyst. *Journal of Industrial and Engineering Chemistry*, 46356-363. <https://doi.org/https://doi.org/10.1016/j.jiec.2016.11.004>
- [31] Wang X, Xu W, Liu N, Yu Z, Li Y and Qiu J (2015) Synthesis of metallic Ni-Co/graphene catalysts with enhanced hydrodesulfurization activity via a low-temperature plasma approach. *Catalysis Today*, 256203-208. <https://doi.org/https://doi.org/10.1016/j.cattod.2015.04.026>
- [32] Weiss W, Guibard I and Dastillung R (2018) Process for hydroconverting oil feeds in fixed beds for the production of low sulphur fuels. In: Google Patents
- [33] Xing T, Alvarez-Majmutov A and Chen J (2019) Bitumen partial upgrading by mild hydroprocessing in a fixed-bed reactor. *Fuel*, 235696-702. <https://doi.org/https://doi.org/10.1016/j.fuel.2018.08.058>
- [34] Yang L, Wang X, Liu Y, Yu Z, Li R and Qiu J (2017) Layer-dependent catalysis of MoS₂/graphene nanoribbon composites for efficient hydrodesulfurization. *Catalysis Science & Technology*, 73: 693-702. <https://doi.org/DOIhttps://doi.org/10.1039/C6CY02074G>
- [35] Yuan L, Wang X, Zhao K, Pan H, Li Q, Yang J and Zhang Z (2017) Effect of reaction temperature and hydrogen donor on the Ni₀@ graphene-catalyzed viscosity reduction of extra heavy crude oil. *Petroleum Science and Technology*, 352: 196-200. <https://doi.org/https://doi.org/10.1080/10916466.2016.1241805>
- [36] Yusefabad E T, Tavasoli A and Zamani Y (2018) Effective catalyst to produce naphtha from vacuum gasoil hydrocracking and discrete lump modeling. *Petroleum & Coal*, 601. <https://doi.org/Corpus ID: 195890031>
- [37] Bamdadi M, Bozorg A, Tavasoli A, Shateri S, Andache M (2019) Synthesis of Meso/Macroporous γ - Alumina via Aluminum Pellet with Controllable Porosity: Ammonium Bicarbonate Influences through Drying and Calcination Steps. *Chemistry Select* 4 (19), 5872-5879. <https://doi.org/10.1002/slct.201900523>
- [38] Hashemi H, Behnejad H, Rosendahl, L Tavasoli A (2022) Tuning the porosity and physicochemical properties of SBA-15: RSM-assisted optimizing of traditional sol-gel process , *Chemical Papers vol 76*, 4541-4560. <https://doi.org/10.1007/s11696-022-02187-z>
- [39] Salimi M, Tavasoli A, Rosendahl L (2020) Optimization of γ -alumina porosity via response surface methodology: the influence of engineering support on the performance of a residual oil hydrotreating catalyst, *Microporous and Mesoporous Materials* 299, 110124. <https://doi.org/10.1016/j.micromeso.2020.110124>

[40] B. Liu, H. Lv, X. Cui, G. Sun, X. Zhang, B. Dong, Y. Li, Y. Pan, Y. Chai, C. Liu, Preparation of presulfided oil-soluble NiMo catalyst for slurry bed hydrocracking of vacuum residue, *Chemical Engineering Journal*, 498 (15), 2024. <https://doi.org/10.1016/j.cej.2024.155166>

[41] D. Dhaneswara, J. Fatriansyah, T. Sudiro, S. Harjanto, M. S. Mastuli, A. Federico, R. Ulfiati, Synthesis and optimization of Ni/Mo-impregnated kaolin-based ZSM-5 as a catalytic hydrocracking catalyst for heavy petroleum distillates, *Sustainable Energy & Fuels*, 12, 2024. <https://doi.org/10.1039/d3se01573d>

[42] K.K. Ferreira, C. Di Stasi, A. Ayala-Cortés, L.S. Ribeiro, J.L. Pinilla, I. Suelves, M.F.R. Pereira, Hydroprocessing of waste cooking oil to produce liquid fuels over Ni-Mo and Co-Mo supported on carbon nanotubes, *Biomass and Bioenergy*, 91, 2024. <https://doi.org/10.1016/j.biombioe.2024.107480>

Accepted Manuscript